Critical point phase transition for finite temperature 3-flavor QCD with nonperturbatively O(a) improved Wilson fermions at Nt=10

doi: 10.1103/PhysRevD.96.034523

Critical point phase transition for finite temperature 3-flavor QCD with nonperturbatively O(a) improved Wilson fermions at $N_t = 10$

Xiao-Yong Jin,[1] Yoshinobu Kuramashi,[2,3] Yoshifumi Nakamura,[3,4] Shinji Takeda,[5,3,*] and Akira Ukawa[3]

[1]*Argonne Leadership Computing Facility, Argonne National Laboratory, Argonne, Illinois 60439, USA*
[2]*Center for Computational Sciences, University of Tsukuba, Tsukuba, Ibaraki 305-8577, Japan*
[3]*RIKEN Advanced Institute for Computational Science, Kobe, Hyogo 650-0047, Japan*
[4]*Graduate School of System Informatics, Department of Computational Sciences, Kobe University, Kobe, Hyogo 657-8501, Japan*
[5]*Institute of Physics, Kanazawa University, Kanazawa 920-1192, Japan*

(Received 6 June 2017; published 30 August 2017)

We study the finite temperature phase structure for three-flavor QCD with a focus on locating the critical point, which separates the crossover and the first order phase transition region in the chiral regime of the Columbia plot. In this study, we employ the Iwasaki gauge action and the nonperturvatively O(a) improved Wilson-Clover fermion action. We discuss the finite size scaling analysis, including the mixing of magnetizationlike and energylike observables. We carry out the continuum extrapolation of the critical point using newly generated data at the $N_t = 8$, 10 and estimate the upper bound of the critical pseudoscalar meson mass $m_{PS,E} \lesssim 170$ MeV and the critical temperature $T_E = 134(3)$ MeV. Our estimate of the upper bound is derived from the existence of the critical point as an edge of the first order phase transition while that of the staggered-type fermions with smearing is based on its absence.

DOI: 10.1103/PhysRevD.96.034523

I. INTRODUCTION

The nature of finite temperature transition in QCD varies depending on the quark masses. A pictorial representation is often given as the Columbia plot [1–3] whose axes are usually taken to be the up-down and strange quark masses. See reviews [4,5] for a current status of the QCD phase structure with the finite temperature and quark number density. In this paper, we restrict ourselves to the case of a zero quark number density.

There are two long-standing issues on the Columbia plot, namely the location of the critical line, which separates the first order phase transition region from the crossover region, and the universality class of the critical line. Studies with the standard staggered fermion action [6–9] successfully located the critical point along the flavor symmetric line ($N_f = 3$). It was subsequently found that the first order region rapidly shrinks towards the continuum limit [10]. Further studies with staggered fermions with smearing techniques [11–13] could not even detect a critical point, perhaps due to the possibility that the critical quark mass is so small that current computational resources cannot access it.

On the other hand, the pioneering Wilson-type fermion study in Ref. [14] reported a relatively heavy critical mass. Our recent study [15], while confirming a large value for coarse lattice spacings, suggested that the critical mass appears to be smaller for finer lattice spacings. This implies that the removal of a scaling violation is crucial for the Wilson-type fermion action as well. In Ref. [15], we computed the critical point for $N_f = 3$ QCD at temporal lattice sizes $N_t = 4$, 6, and 8. In order to take the continuum limit more reliably, we have recently started large scale simulations at $N_t = 10$, and preliminary results were already reported in the previous lattice conferences [16,17]. In this paper, we finalize the analysis including the new data, which consists of one additional β value with $N_t = 8$ and a totally new data set of $N_t = 10$, and examine the continuum limit with the added data.

Concerning the issue with the universality class along the critical line, we observed in Refs. [15,16] that for $N_t = 8$ and 10, the values of the kurtosis from different volumes intersect at a point away from the three-dimensional Z_2 universality class, in contrast to the situation with $N_t = 4$ and 6, where they are consistent. We address this issue by noting that bare lattice observables generally are mixtures of magnetizationlike and energylike operators; this should be taken into account in finite size scaling analyses.

The rest of the paper is organized as follows. In Sec. II, we review the kurtosis intersection analysis and then discuss the finite size correction for kurtosis of an observable, which has a nontrivial overlap with the energylike operator, around the critical point. After describing the simulation setup in Sec. III, we locate the critical point by applying the new fitting formulas in a kurtosis intersection analysis and then take the continuum limit of the critical point in Sec. IV. Our conclusions are summarized in Sec. V. Results of zero temperature simulations for scale setting are summarized in the Appendix.

*takeda@hep.s.kanazawa-u.ac.jp

II. SCALING ANALYSIS FOR GENERAL OBSERVABLE

In this section, we review the standard kurtosis intersection formula and derive a new formula which incorporates the finite volume effect for kurtosis of a general observable, which is a mixture of an energylike and magnetizationlike operator around the critical point. The mixed observable analysis was originally discussed and demonstrated in Ref. [7], where, first of all, the magnetization part is extracted by using some observables and then the kurtosis intersection analysis is applied to the magnetization-dominated observable. Here, however, we consider a general observable without purifying the magnetization part and derive a formula of the kurtosis with the correction term originating from the energylike operator part. The derived formula will be used in the subsequent analysis.

In a scaling analysis, the relevant parameters are reduced temperature t, external magnetic field h, and the inverse of the linear lattice size L^{-1}. According to the finite size scaling theory, under scaling by a factor b, the free energy (not free energy density) scales as follows up to the analytic terms:

$$F(t,h,L^{-1}) = F(tb^{y_t}, hb^{y_h}, L^{-1}b), \tag{1}$$

where y_t and y_h are the exponent for the temperature and the magnetic field, respectively. Setting $b = L$, the scaling relation of the free energy is given by

$$F(t,h,L^{-1}) = F(tL^{y_t}, hL^{y_h}, 1). \tag{2}$$

In the following, we use the notation and abbreviation below:

$$F(tL^{y_t},0,1) = F(tL^{y_t}),$$
$$\frac{\partial^n}{\partial t^n}\frac{\partial^m}{\partial h^m}F(t,h,L^{-1}) = F^{(nm)}(t,h,L^{-1}). \tag{3}$$

As an explicit and well-known example, first we consider the purely magnetic observable $\mathcal{M}$, whose moments can be obtained by applying the derivative in terms of h to the free energy

$$\mathcal{M} \to \frac{\partial}{\partial h}. \tag{4}$$

The susceptibility for $\mathcal{M}$ at $h = 0$ is given by

$$\begin{aligned}\chi_{\mathcal{M}}(t,0,L^{-1}) &= L^{-d}\frac{\partial^2 F(t,h,L^{-1})}{\partial h^2}\bigg|_{h=0} \\ &= L^{-d+2y_h}F^{(02)}(tL^{y_t},0,1) \\ &= L^{-d+2y_h}F^{(02)}(tL^{y_t}),\end{aligned} \tag{5}$$

where d is the dimension of the system. As is well-known, the susceptibility at $t = 0$ scales as (using $-d + 2y_h = \gamma/\nu$)

$$\chi_{\mathcal{M}}(0,0,L^{-1}) \propto L^{\gamma/\nu}. \tag{6}$$

The kurtosis for $\mathcal{M}$ at $h = 0$ is given by

$$\begin{aligned}K_{\mathcal{M}}(t,0,L^{-1}) &= \frac{F^{(04)}(t,h,L^{-1})|_{h=0}}{[F^{(02)}(t,h,L^{-1})|_{h=0}]^2} \\ &= \frac{L^{4y_h}F^{(04)}(tL^{y_t})}{[L^{2y_h}F^{(02)}(tL^{y_t})]^2} = \frac{F^{(04)}(tL^{y_t})}{[F^{(02)}(tL^{y_t})]^2}.\end{aligned} \tag{7}$$

At a critical point, the kurtosis is independent of the volume. For small tL^{y_t}, one can expand

$$K_{\mathcal{M}}(t,0,L^{-1}) = \frac{F^{(04)}(0)}{[F^{(02)}(0)]^2} + c_K tL^{1/\nu} + \cdots, \tag{8}$$

where we have used $y_t = 1/\nu$. This is the well-known formula for the kurtosis intersection analysis.

For a general observable $\mathcal{O}$, which is a mixture of energy $\mathcal{E}$ and magnetization $\mathcal{M}$,

$$\mathcal{O} = c_M\mathcal{M} + c_E\mathcal{E} \to c_M\frac{\partial}{\partial h} + c_E\frac{\partial}{\partial t}, \tag{9}$$

the susceptibility and kurtosis of $\mathcal{O}$ at $h = 0$ are given by

$$\begin{aligned}\chi_{\mathcal{O}}(t,0,L^{-1}) &= L^{-d}\left(c_M\frac{\partial}{\partial h} + c_E\frac{\partial}{\partial t}\right)^2 F(t,h,L^{-1})\Big|_{h=0} \\ &= L^{-d+2y_h}c_M^2\Bigg[F^{(02)}(tL^{y_t}) \\ &\quad + 2\frac{c_E}{c_M}L^{y_t-y_h}F^{(11)}(tL^{y_t}) + O(L^{2(y_t-y_h)})\Bigg],\end{aligned} \tag{10}$$

$$\begin{aligned}K_{\mathcal{O}}(t,0,L^{-1}) &= \frac{(c_M\frac{\partial}{\partial h} + c_E\frac{\partial}{\partial t})^4 F(t,h,L^{-1})|_{h=0}}{[(c_M\frac{\partial}{\partial h} + c_E\frac{\partial}{\partial t})^2 F(t,h,L^{-1})|_{h=0}]^2} \\ &= \frac{F^{(04)}(tL^{y_t})}{F^{(02)}(tL^{y_t})^2}\Bigg[1 + \frac{4c_E}{c_M}L^{y_t-y_h}\left(\frac{F^{(13)}(tL^{y_t})}{F^{(04)}(tL^{y_t})}\right. \\ &\quad \left. - \frac{F^{(11)}(tL^{y_t})}{F^{(02)}(tL^{y_t})}\right) + O(L^{2(y_t-y_h)})\Bigg].\end{aligned} \tag{11}$$

Thus, even when setting $t = 0$, the correction term of $O(c_E L^{y_t-y_h}/c_M)$ remains[1]. In particular, the correction term alters the value of the kurtosis at the critical point. The difference of the exponents $y_t - y_h$ is usually negative for various universality classes, *viz.*

[1]For the kurtosis, there is another correction term originated from the irrelevant scaling field $N_s^{-1/\nu-\omega}$. The value of ω for three-dimensional Z_2 universality class is 0.83… and the magnitude of the correction term is similar to that of the mixing. In numerical analysis it is hard to disentangle them. Therefore in this paper, we deal with only the dominant mixing correction term and just ignore the irrelevant contribution. We thank de Forcrand for reminding us this issue.

$$y_t - y_h = \frac{1}{2\nu}(\alpha - \gamma) = \begin{cases} \frac{1}{2\cdot 1}(0 - 7/4) & = -7/8 \quad : \text{2D Ising}, \\ \frac{1}{2\cdot 0.630}(0.110 - 1.237) & = -0.894 \quad : \text{3D Ising}, \\ \frac{1}{2\cdot 0.67}(-0.01 - 1.32) & = -0.993 \quad : \text{3D O(2)}, \\ \frac{1}{2\cdot 0.75}(-0.25 - 1.47) & = -1.15 \quad : \text{3D O(4)}. \end{cases} \tag{12}$$

Therefore, such a correction would be irrelevant in the large volume limit. However, at finite volumes, the value of the kurtosis at $t = 0$ has a volume dependence; the kurtosis for various volumes would not cross at a single point.

III. SETUP AND METHODS

We employ the Iwasaki gauge action [18] and nonperturvatively O(a) improved Wilson-Clover fermion action [19] to carry out the finite temperature $N_f = 3$ QCD simulation. The temporal lattice size we newly report here is a part of $N_t = 8$ and all $N_t = 10$ data. For $N_t = 8$ and 10, the spatial lattice size is varied over $N_s = 16$, 20, 24, and 28 to carry out the finite size scaling. BQCD code [20] implementing the RHMC algorithm [21] is used to generate gauge configurations, with the acceptance rate tuned to be around 80%. We store configurations at every tenth trajectory for observable measurements. Since the three dynamical quarks are all degenerate, we have only one hopping parameter κ. Some values of the parameter β are selected, and κ is adjusted to search for a transition point at each β. See Table I for the parameter sets and their statistics. The new β value for $N_t = 8$, which was absent in [15], is $\beta = 1.745$.

TABLE I. Simulation parameters and the number of configurations for $N_t = 8$ and 10.

N_t	β	κ	$N_s = 16$	$N_s = 20$	$N_s = 24$	$N_s = 28$
8	1.745	0.140371	5600	3050	850	400
		0.140380	6170	7890	×	×
		0.140382	×	×	11 200	11 830
		0.140384	×	×	×	6670
		0.140385	×	9910	15 700	×
		0.140393	14 570	×	×	×
	1.74995	0.140240	15 498	10 700	9700	6580
	1.76019	0.139950	16 650	11 230	10 560	×
10	1.77	0.139800	640	×	×	×
		0.139820	1620	×	×	×
		0.139830	1520	×	×	×
		0.139850	3510	2000	×	×
		0.139855	×	2410	830	×
		0.139857	×	×	380	×
		0.139858	×	×	710	×
		0.139860	×	2500	630	×
		0.139870	3590	×	×	×
		0.139900	760	×	×	×
	1.78	0.139550	1220	×	×	×
		0.139560	1520	×	×	×
		0.139580	2720	×	×	×
		0.139600	2870	×	×	×
		0.139610	2640	1640	720	×
		0.139615	×	3810	2320	1610
		0.139620	2460	4400	2360	1110
		0.139625	×	690	550	×
		0.139630	×	490	×	×
		0.139650	1790	×	×	×
	1.79	0.139300	2760	×	×	×
		0.139325	2710	×	×	×
		0.139340	×	2660	730	×
		0.139350	3270	2380	960	×
		0.139400	3460	×	×	×

The details of our analysis method can be found in our previous studies [15,22], and we summarize it in the following.

We use the naive chiral condensate as a probe to study the phase structure. We measure higher moments of the chiral condensate up to the fourth order to calculate the susceptibility, the skewness, and the kurtosis equivalent to the Binder cumulant up to an additional constant. In order to determine the transition point, we use the peak position of the susceptibility and verify that it coincides with the zero of the skewness. The kurtosis is used to locate the critical point through the intersection analysis [7] with our extension discussed in the previous section.

We combine several ensembles, which share common parameter values except for κ, by the multiensemble reweighting [23] in κ for interpolating the moments. We do not apply β reweighting. To calculate the reweighting factor given by the ratio of fermion determinants at different κ values, we use an expansion of the logarithm of the determinant [22]. For the computation of the observable part in the reweighting procedure, we need to evaluate quark propagators at continuously many points of κ. We adopt an expansion form for the moments which allows us to evaluate the moments at continuously many points at a relatively low cost. The multiensemble reweighting is applied to the data at $N_t = 8$ and 10 as well as the old $N_t = 4$, 6 data without adding the new data set. For all values of N_t, our parameter sets satisfy $m_{PS}L \gtrsim 4$, where m_{PS} is the pseudoscalar meson mass.

IV. RESULTS

A. Moments and location of the transition point

As an illustration of the new data, we show the susceptibility and the kurtosis of the chiral condensate for $(N_t, \beta) = (8, 1.745)$ and $(N_t, \beta) = (10, 1.78)$ in Fig. 1 together with the κ-reweighting results. From the peak position of the

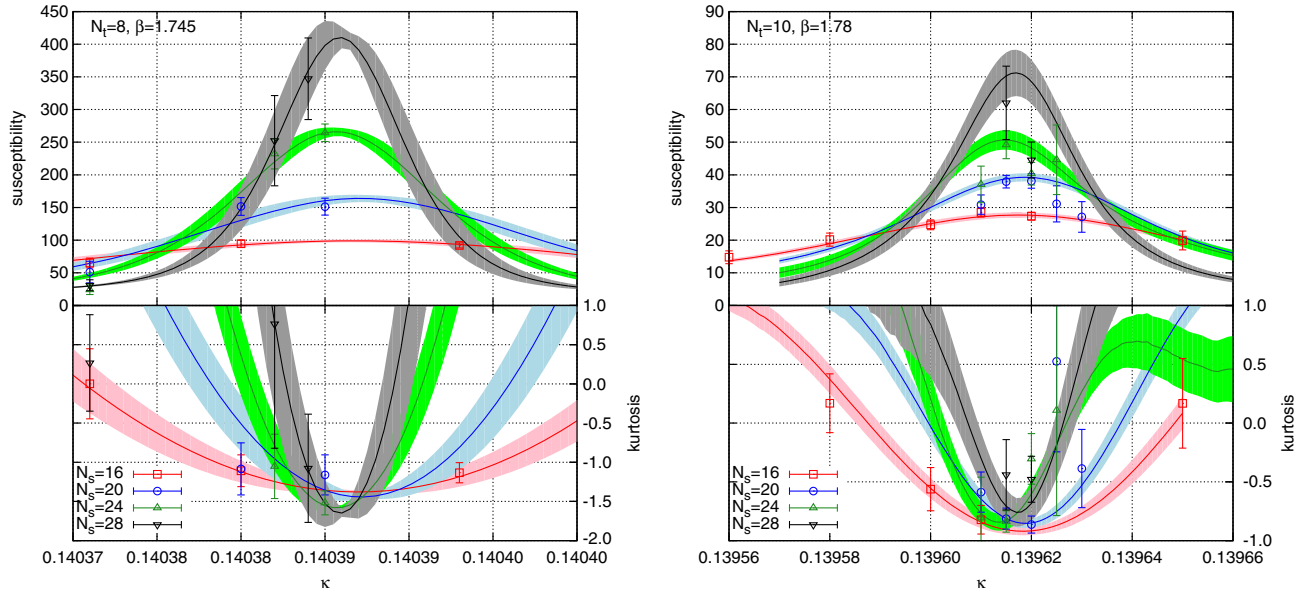

FIG. 1. The susceptibility (upper half) and kurtosis (lower half) of chiral condensate as a function κ with several spatial sizes, $N_s = 16$–28. The left panel is for $(N_t, \beta) = (8, 1.745)$ and the right is for $(N_t, \beta) = (10, 1.78)$. The raw data points (as symbols) as well as the multiensemble reweighting ($1 - \sigma$ band) are plotted.

susceptibility, we extract the transition points. The thermodynamic limit of the transition point is taken by using a fitting form with an inverse spatial volume correction term. The resulting phase diagram in the bare parameter space is summarized in Fig. 2. Polynomial interpolation is used to determine the phase transition line.

B. Kurtosis analysis

The minimum of kurtosis at each (N_s, β) is plotted in Fig. 3 to perform kurtosis intersection analysis at $N_t = 4$, 6, 8, and 10. Although $N_t = 4$ and 6 results clearly show that the critical universality class is consistent with the 3D Z_2 universality class, for $N_t = 8$ and 10 an analysis using the

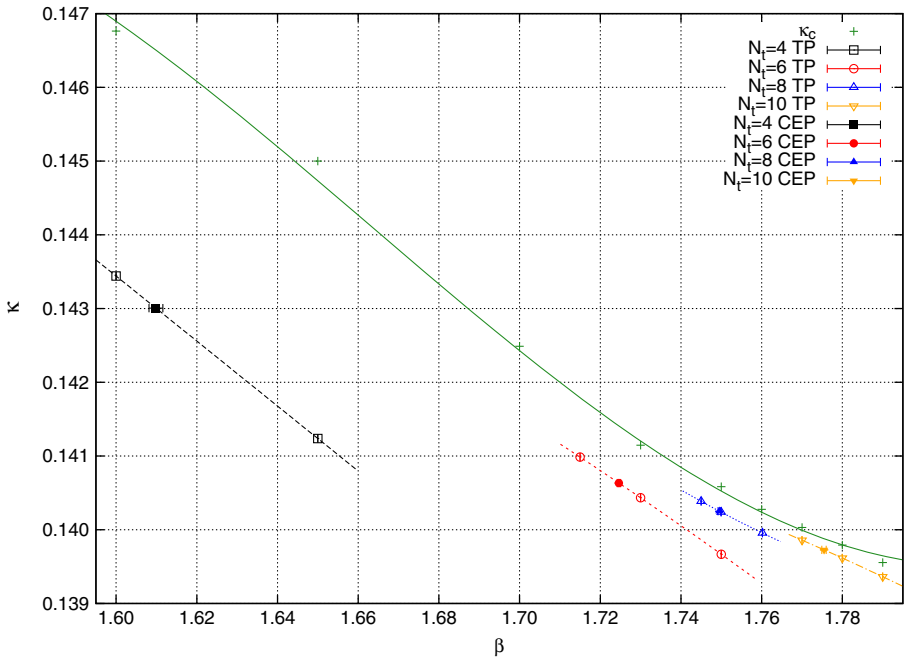

FIG. 2. Phase diagram for bare parameter space (β, κ) at $N_t = 4$, 6, 8, and 10. The open symbols represent a transition/crossover point while the filled symbols are the critical end points determined by the kurtosis intersection with a new formula. On the transition line, the left- (right-)hand side of an critical end point is the first order phase transition (crossover) side. Polynomial interpolation is used to determine the phase transition line. κ_c is the pseudoscalar massless point with $N_f = 3$ at the zero temperature.

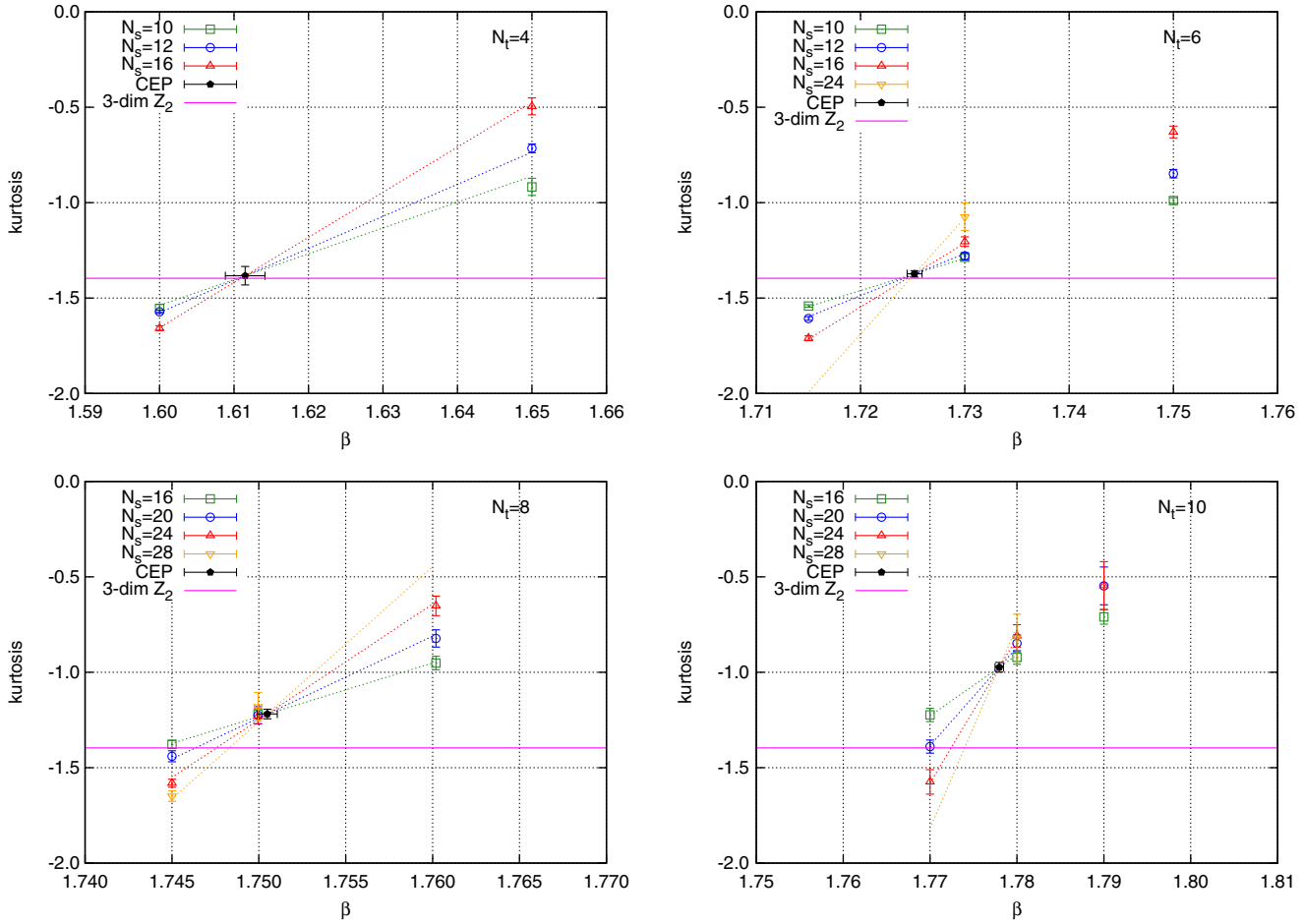

FIG. 3. Kurtosis intersection for chiral condensate at $N_t = 4$, 6, 8, and 10. The simple fitting form: $K = K_E + AN_s^{1/\nu}(\beta - \beta_E)$ is also drawn in the figure. For $N_t = 4$ and 6, the values of kurtosis at the crossing point (black pentagon) is consistent with the three-dimensional Z_2 universality class, while for $N_t = 8$ and 10, obviously, it is not consistent. The conclusion of this paper is based on the fitting form with a correction term. See text for details.

conventional formula as Eq. (8) leads to a value for K_E, which is substantially larger than that for the universality class. In this situation, we attempt a modified fitting form that incorporates the correction term in Eq. (11) associated with the contribution of the energylike observable given by

$$K = [K_E + AN_s^{1/\nu}(\beta - \beta_E)](1 + BN_s^{y_t - y_h}), \qquad (13)$$

where we have two additional parameters B and $y_t - y_h$. We have tried three fits. Fit 1 has no correction term ($B = y_t - y_h = 0$), and all other parameters are used as fit parameter. Fit 2 also neglects the correction term assuming the 3D Z_2 universality class for K_E and ν. Fit 3 includes the correction term assuming the 3D Z_2 universality class for K_E, ν and $y_t - y_h$. The fit results are summarized in Table II.

For $N_t = 4$ and 6, the parameter B in the Fit 3 is consistent with zero, and all other fitting parameters of all fitting forms are consistent with each other. Thus, we conclude that the new correction term is negligible, and the universality class is consistent with 3D Z_2 for $N_t = 4$ and 6.

For $N_t = 8$ and 10, the assumption of a Z_2 universality class is unlikely to hold without the new correction term since the Fit 2, which assumes the Z_2 values for K_E and ν have a large χ^2/d.o.f. On the other hand, with the Fit 3 assuming Z_2 but including the correction term from the mixing of magnetization and energy terms, we observe a reasonable χ^2/d.o.f. < 1. The magnitude of the correction term, $BN_s^{y_t - y_h}$, is reasonably small, of an order of 10%. This suggests that $N_t = 8$ and 10 results are consistent with the 3D Z_2 universality class if one includes the correction term.

In the following, we adopt the critical point β_E determined by the Fit 3 (assuming a 3D Z_2 universality class with the correction term). The corresponding critical value of κ, that is, κ_E is estimated by an interpolated transition line as in Fig. 2, where the critical point in the bare parameter space (β, κ) is shown.

C. Cross-check using exponent of the susceptibility peak height

For a cross-check of the location and the universality class of the critical point, we investigate the scaling of the susceptibility peak height for the chiral condensate,

$$\chi_{max} \propto (N_s)^b. \qquad (14)$$

TABLE II. Fit results for kurtosis intersection with fitting form in Eq. (13). See text for the definition of Fits 1, 2, and 3. A value without an error bar means that the corresponding fit parameter is fixed to the given value during the fit. For the 3D Z_2 universality class, the expected values of the parameter are $K_E = -1.396$, $\nu = 0.630$, and $y_t - y_h = -0.894$, respectively. Using the value of β_E as an input, κ_E is obtained from an interpolation formula of the transition line in Fig. 2.

N_t	Fit	β_E	κ_E	K_E	ν	A	B	$y_t - y_h$	χ^2/d.o.f.
4	1	1.6115(26)	0.1429337(13)	−1.383(48)	0.84(13)	0.88(42)	×	×	1.75
	2	1.61065(61)	0.1429713(13)	−1.396	0.63	0.313(12)	×	×	3.05
	3	1.6099(17)	0.1430048(13)	−1.396	0.63	0.311(14)	0.10(21)	−0.894	3.77
6	1	1.72518(71)	0.1406129(14)	−1.373(17)	0.683(54)	0.58(17)	×	×	0.68
	2	1.72431(24)	0.1406451(14)	−1.396	0.63	0.418(11)	×	×	0.70
	3	1.72462(40)	0.1406334(14)	−1.396	0.63	0.422(12)	−0.052(52)	−0.894	0.70
8	1	1.75049(57)	0.1402234(11)	−1.219(25)	0.527(55)	0.146(88)	×	×	0.73
	2	1.74721(42)	0.14031921(76)	−1.396	0.63	0.404(36)	×	×	5.99
	3	1.74953(33)	0.1402512(10)	−1.396	0.63	0.414(13)	−1.33(15)	−0.894	0.73
10	1	1.77796(48)	0.1396661(17)	−0.974(25)	0.466(45)	0.084(52)	×	×	0.22
	2	1.7694(16)	0.1398724(22)	−1.396	0.63	0.421(95)	×	×	10.03
	3	1.77545(53)	0.1397274(17)	−1.396	0.63	0.559(29)	−2.97(25)	−0.894	0.43

At a critical point, the exponent should be $b = \gamma/\nu$ as in Eq. (6). For a general observable, the dominant part shows the same scaling as in Eq. (14), while a correction term as in Eq. (10) remains even at the critical point. For a qualitative verification, we neglect the correction term and extract the exponent b with a log-linear fit. The resulting exponent b is plotted in Fig. 4 along the transition line projected on β. Assuming the Z_2 universality class provides an estimation of the critical point of β, we confirm that it is consistent with that of the kurtosis intersection. This cross-check assures that our analysis is working well.

D. Continuum extrapolation of critical pseudoscalar meson mass and critical temperature

Before taking the continuum limit, let us summarize the dimensionless combination of the pseudoscalar meson mass m_{PS}, the Wilson flow scale $\sqrt{t_0}$ [24], and the temperature T along the transition line in Fig. 5. They are calculated by zero temperature simulations, and their results are summarized in the Appendix. The zero temperature simulation covers the parameter range of the critical points. From an interpolation or a short extrapolation, one can obtain the critical value of the dimensionless quantities for each temporal size N_t. The actual numbers are summarized in Table III.

Finally, in Fig. 6 (upper-left and lower-left panels), we show the continuum extrapolation of the critical pseudoscalar meson mass $\sqrt{t_0}m_{PS,E}$ and the critical temperature $\sqrt{t_0}T_E$ normalized by $\sqrt{t_0}$. The latter shows a stable continuum extrapolation, and we obtain $\sqrt{t_0}T_E = 0.09932(39)$. The critical temperature in physical units is given by $T_E = 134(3)$ MeV using the Wilson flow scale $1/\sqrt{t_0} = 1.347(30)$ GeV in Ref. [25]. On the other hand $\sqrt{t_0}m_{PS,E}$ shows significantly large scaling violation. In the

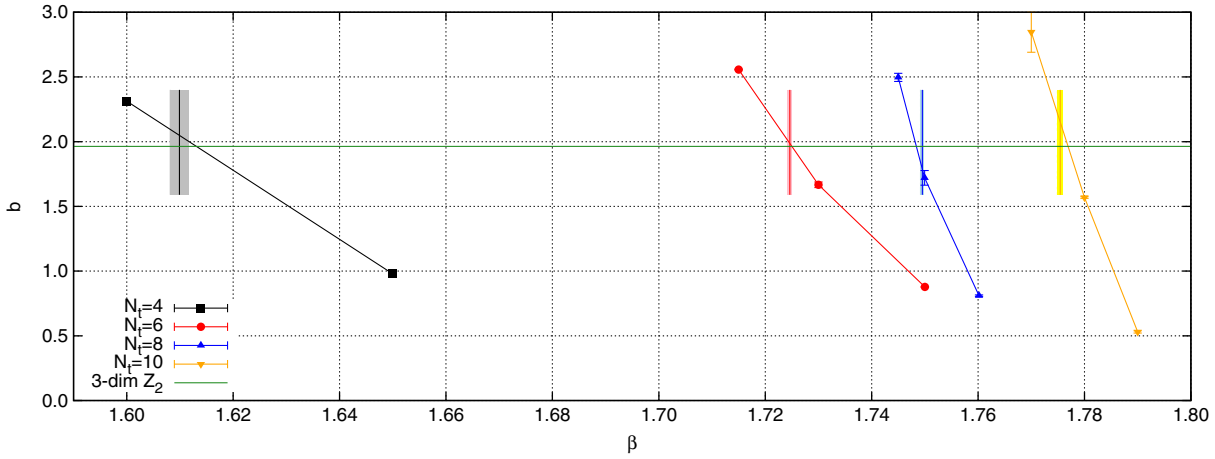

FIG. 4. Exponents of the susceptibility peak height along the transition line projected on β value for $N_t = 4$, 6, 8, and 10. The line connecting the data points is to guide the readers' eyes. The point where the line for each N_t intersects the (green) horizontal line is an estimate of the critical point assuming the Z_2 universality class. On the other hand, the shaded areas represent the critical β determined by the kurtosis intersection analysis.

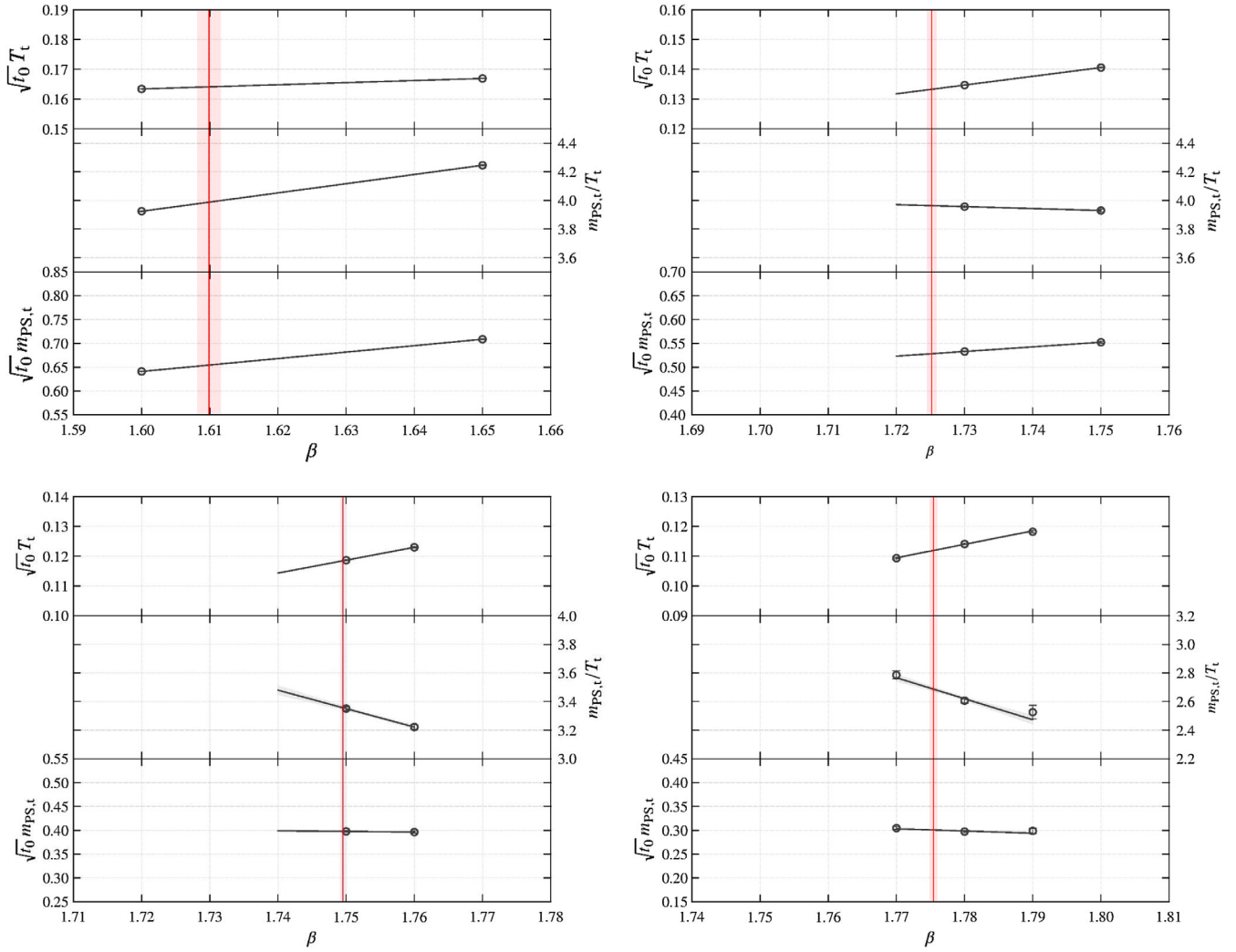

FIG. 5. $\sqrt{t_0}T$, m_{PS}/T, and $\sqrt{t_0}m_{PS}$ along the transition line projected on β for $N_t = 4$ (upper left), 6 (upper right), 8 (lower left), and 10 (lower right). The vertical red line shows the location of the critical value of β determined by the kurtosis intersection analysis.

extrapolation procedure, we try some fitting forms including up to a cubic correction term and examine the fitting range dependence. As a result, their dependence turns out to be large as shown in Fig. 6 (upper left) and Table III. Furthermore, we investigate the critical mass in terms of the quark mass like quantity, $(\sqrt{t_0}m_{PS,E})^2 \propto m_q$ in Fig. 6 (upper right). The result shows the large scaling violation as well and extrapolates to a negative value in the continuum limit. The inconsistency of the continuum value for $\sqrt{t_0}m_{PS,E}$ and $(\sqrt{t_0}m_{PS,E})^2$, in particular their signature, indicates that the part of our data with $N_t = 4$–10 may not be in the scaling region. Therefore, here we conservatively quote an upper bound of the critical value $\sqrt{t_0}m_{PS,E} \lesssim 0.13$. The value of the upper limit is taken from the maximum continuum value among all the fits we did. In physical units, this bound is $m_{PS,E} \lesssim 170$ MeV. This upper bound is much smaller than our previous estimate (∼300 MeV) [15]; the reason being that the latest point at $N_t = 10$ (see Fig. 6) bends down toward the continuum extrapolation.

TABLE III. The hadronic dimensionless quantities at the critical point for $N_t = 4$, 6, 8, and 10, and their continuum extrapolation with various fitting ranges and fitting forms.

N_t	$\sqrt{t_0}m_{PS,E}$	$\sqrt{t_0}T_E$	$m_{PS,E}/T_E$
4	0.6545(24)	0.16409(13)	3.987(12)
6	0.5282(12)	0.13328(23)	3.9630(63)
8	0.3977(19)	0.11845(20)	3.357(16)
10	0.3006(19)	0.11193(29)	2.687(18)
∞ (fit)	0.0938(39)	0.09970(37)	0.941(39)
∞ (solve and quadratic)	0.1281(61)	⋯	1.285(61)
∞ (solve and cubic)	0.039(14)	⋯	0.39(14)

For future references, we address the continuum extrapolation of $m_{PS,E}/T_E$. As shown in Fig. 6 (lower right), the lattice cutoff dependence is quite large, and in fact, the continuum extrapolation was not smoothly taken. Therefore, instead of performing a direct continuum extrapolation of $m_{PS,E}/T_E$, we take a ratio of the two values of $\sqrt{t_0}m_{PS,E}$ and

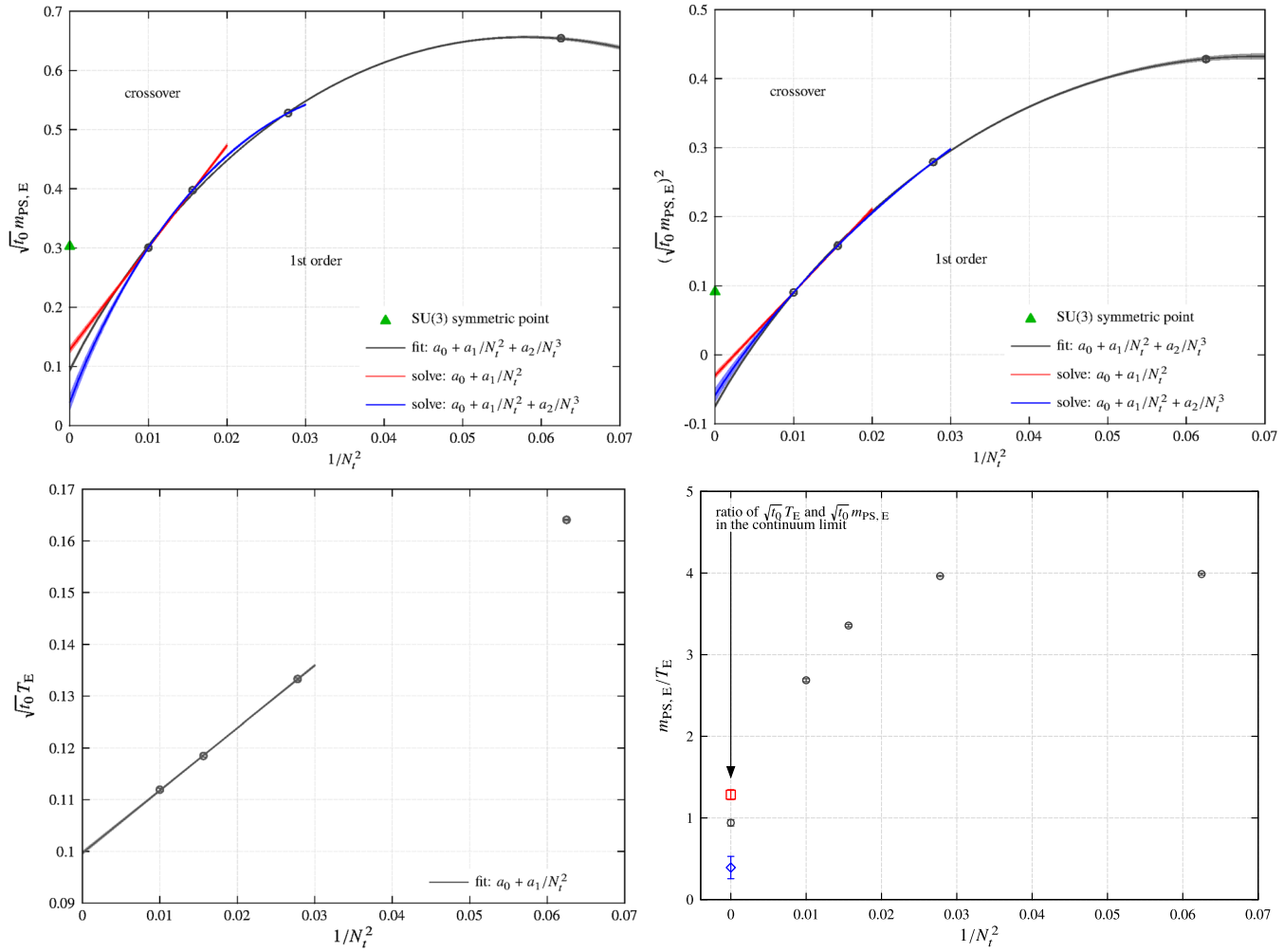

FIG. 6. Continuum extrapolation of the critical point $\sqrt{t_0}m_{\mathrm{PS,E}}$ (upper left), $(\sqrt{t_0}m_{\mathrm{PS,E}})^2$ (upper right), $\sqrt{t_0}T_{\mathrm{E}}$ (lower left), and $m_{\mathrm{PS,E}}/T_{\mathrm{E}}$ (lower right). Note that the continuum value of $m_{\mathrm{PS,E}}/T_{\mathrm{E}}$ in the lower-right panel is obtained by using the ratio of $\sqrt{t_0}m_{\mathrm{PS,E}}$ and $\sqrt{t_0}T_{\mathrm{E}}$ in the continuum limit obtained in the upper-left and the lower-left panels, respectively.

$\sqrt{t_0}T_{\mathrm{E}}$ at the continuum limit and then obtain the upper bound $m_{\mathrm{PS,E}}/T_{\mathrm{E}} \lesssim 1.3$.

V. SUMMARY AND OUTLOOK

We carried out the large scale simulations for $N_{\mathrm{t}} = 10$ and partly, $N_{\mathrm{t}} = 8$ by using the Wilson-type fermions. This is an extension of the previous work at $N_{\mathrm{t}} = 4$, 6, and 8 [15]. We observed that the value of kurtosis at the crossing point tends to be larger as N_{t} increases. To resolve the issue, we derive and apply the modified formula to the kurtosis intersection analysis. By using the formula, the critical point is determined with assuming a 3D Z_2 universality class. We estimate the upper bound of the critical point and its temperature as

$$m_{\mathrm{PS,E}} \lesssim 170\ \mathrm{MeV}, \tag{15}$$

$$T_{\mathrm{E}} = 134(3)\ \mathrm{MeV}, \tag{16}$$

$$m_{\mathrm{PS,E}}/T_{\mathrm{E}} \lesssim 1.3. \tag{17}$$

Note that the continuum extrapolation significantly dominates the systematic error; thus, we compromise to quote the upper bound of $m_{\mathrm{PS,E}}$. Since we are using the value of c_{sw} at a very low β which is out of the interpolation range [19], it may be possible that the $\mathrm{O}(a)$ improvement program is not properly working in our parameter region. In order to control the lattice cutoff effect, one can straightforwardly extend the temporal lattice size N_{t} but its cost is very demanding. Another possibility may be to redo the same calculation with a different lattice action, say a different gauge action but the same/similar Wilson-type fermions. And then one can perform a combined fit with an additional estimate of the critical point.

Our estimate of the upper bound of $m_{\mathrm{PS,E}}$ is larger than that obtained by the staggered type fermions [13], $m_{\mathrm{PS,E}} \lesssim 50$ MeV. Note that, however, our upper bound is derived from the existence of the critical point as an edge of the first order phase transition while the estimate of the staggered study was based on its absence. For $m_{\mathrm{PS,E}}/T_{\mathrm{E}}$, our bound is consistent with the result of the standard staggered fermions [10,26], $m_{\mathrm{PS,E}}/T_{\mathrm{E}} = 0.37$.

Although our results of Wilson-type fermions is consistent with that of staggered-type fermions, it is premature to conclude that the universality is confirmed. In the future, as errors reduce, a discrepancy may appear. As seen above, the Wilson-type fermion is suffering from the large cutoff effects; on the other hand, the staggered fermions with the odd flavors may have trouble in the chiral regime at a finite lattice spacing, namely the rooting issue. Thus, before studying $N_f = 3$ QCD intensively, it is useful to study the universality for $N_f = 4$ QCD [26], where there is no rooting issue and one can purely discuss the universality issue. We are planning to study $N_f = 4$ QCD with Wilson-type fermions.

ACKNOWLEDGMENTS

This research used computational resources of HA-PACS and COMA provided by Interdisciplinary Computational Science Program in the Center for Computational Sciences at the University of Tsukuba, System E at Kyoto University through the HPCI System Research project (Project No. hp150141), PRIMERGY CX400 tatara at Kyushu University and HOKUSAI GreatWave (Project No. G16016) at RIKEN. This work is supported by JSPS KAKENHI Grant No. 26800130, FOCUS Establishing Supercomputing Center of Excellence, and the Kanazawa University SAKIGAKE Project. This research used resources of the Argonne Leadership Computing Facility, which is a DOE Office of Science User Facility supported under Contract No. DE-AC02-06CH11357.

APPENDIX: WILSON FLOW SCALE AND PSEUDOSCALAR MESON MASS AT ZERO TEMPERATURE

Simulation parameters, results for mass of pseudoscalar meson am_{PS}, and Wilson flow scale parameter $\sqrt{t_0}/a$ are summarized in Tables IV and V. Result of following combined fit is given in Table VI:

TABLE IV. Simulation parameters, κ, N_s, N_t, and $\sqrt{t_0}/a$ and am_{PS} at $\beta = 1.60$–1.75.

β	κ	N_s	N_t	$\sqrt{t_0}/a$	am_{PS}
1.60	0.143000	12	24	0.650783(71)	1.02752(71)
	0.143446	12	24	0.653722(72)	0.98078(68)
	0.144000	12	24	0.658485(90)	0.91122(74)
	0.145000	12	24	0.67160(15)	0.7516(13)
1.65	0.140000	12	24	0.659353(65)	1.17770(72)
	0.141240	12	24	0.66818(11)	1.06023(80)
	0.142000	12	24	0.67631(11)	0.96934(88)
	0.143000	12	24	0.69391(21)	0.8111(14)
1.70	0.137100	12	24	0.673734(84)	1.28494(85)
	0.137600	12	24	0.67752(11)	1.24623(92)
	0.138100	12	24	0.68124(11)	1.19924(87)
	0.138250	12	24	0.68277(12)	1.18640(76)
	0.138610	12	24	0.68608(12)	1.15202(69)
	0.140000	16	32	0.705367(99)	0.99132(64)
	0.141000	16	32	0.73207(14)	0.8243(15)
	0.141200	16	32	0.74115(22)	0.77591(83)
	0.141456	16	32	0.75598(23)	0.70619(86)
	0.141800	16	32	1.1510(12)	0.4887(24)
1.73	0.139000	12	24	0.73453(26)	0.96412(97)
	0.139500	12	24	0.75087(27)	0.8833(11)
	0.140000	16	32	0.77484(31)	0.7787(11)
	0.140334	16	32	0.79915(38)	0.68974(85)
	0.140435	16	32	0.80879(42)	0.65851(99)
	0.140500	16	32	0.81630(36)	0.63650(93)
	0.141000	16	32	0.9391(21)	0.3306(45)
1.75	0.139000	12	24	0.79055(42)	0.82237(93)
	0.139500	12	24	0.82671(76)	0.7017(15)
	0.139529	16	32	0.82959(42)	0.69470(91)
	0.139669	16	32	0.84360(53)	0.6569(11)
	0.139700	16	32	0.84799(45)	0.64517(96)
	0.139850	16	32	0.86861(51)	0.59293(89)
	0.140000	16	32	0.8917(14)	0.5355(29)
	0.140242	16	32	0.9508(10)	0.4176(18)

$$(am_{\mathrm{PS}})^2 = a_1\left(\frac{1}{\kappa}-\frac{1}{\kappa_c}\right)+a_2\left(\frac{1}{\kappa}-\frac{1}{\kappa_c}\right)^2, \tag{A1}$$

$$\frac{\sqrt{t_0}}{a} = b_0 + b_1\left(\frac{1}{\kappa}-\frac{1}{\kappa_c}\right)+b_2\left(\frac{1}{\kappa}-\frac{1}{\kappa_c}\right)^2. \tag{A2}$$

TABLE V. Simulation parameters, κ, N_s, N_t, and $\sqrt{t_0}/a$ and am_{PS} at $\beta = 1.76$–1.79.

β	κ	N_s	N_t	$\sqrt{t_0}/a$	am_{PS}
1.76	0.139000	16	32	0.83107(33)	0.73691(77)
	0.139500	16	32	0.88650(51)	0.59667(93)
	0.139800	16	32	0.94019(98)	0.4839(14)
	0.139850	16	32	0.9530(12)	0.4567(17)
	0.139950	16	32	0.9823(13)	0.4060(14)
1.77	0.137100	12	24	0.77014(39)	1.0040(12)
	0.137670	12	24	0.79076(35)	0.91999(86)
	0.138500	12	24	0.83773(53)	0.7675(12)
	0.138700	12	24	0.85652(79)	0.7172(18)
	0.138903	16	32	0.87524(52)	0.66902(80)
	0.139000	16	32	0.88795(57)	0.63966(81)
	0.139653	16	32	1.0096(13)	0.4063(14)
	0.139750	16	32	1.0447(17)	0.3528(20)
	0.139850	16	32	1.0903(34)	0.2851(36)
	0.139900	16	32	1.1163(52)	0.2433(49)
1.78	0.139356	16	32	1.0299(67)	0.4079(21)
	0.139500	16	32	1.0910(20)	0.3340(16)
	0.139600	16	32	1.1306(18)	0.2729(16)
	0.139650	16	32	1.1615(28)	0.2332(22)
1.79	0.139000	16	32	1.0586(22)	0.4253(34)
	0.139200	16	32	1.1158(18)	0.3419(14)
	0.139300	16	32	1.1516(21)	0.2903(21)
	0.139400	16	32	1.2019(28)	0.2270(28)

TABLE VI. Fit results to (A1) and (A2) for critical hopping parameter κ_c and coefficients for pseudoscalar meson mass am_{PS} and Wilson flow parameter $\sqrt{t_0}/a$ for $\beta = 1.60$ to 1.79.

β	κ_c	a_1	a_2	b_0	b_1	b_2	χ^2/d.o.f.	fit range $\kappa >$
1.60	0.146763(36)	7.61(17)	−9.57(74)	0.7064(13)	−0.516(14)	1.149(46)	2.18	0.1430
1.65	0.145000(29)	7.60(11)	−8.01(35)	0.7409(12)	−0.5967(99)	1.079(25)	27.55	0.1400
1.70	0.142488(22)	11.02(25)	−25.2(1.7)	0.8360(26)	−1.926(37)	7.05(18)	2.40	0.1400
1.73	0.1411461(64)	15.62(34)	−98.1(7.5)	0.9944(42)	−8.17(21)	83.2(3.2)	0.90	0.1403
1.75	0.1405835(88)	10.55(25)	−29.0(3.7)	1.0504(41)	−6.59(15)	46.3(1.8)	2.53	0.1395
1.76	0.140276(17)	10.56(62)	−40(12)	1.109(12)	−9.06(65)	87(11)	1.38	0.1395
1.77	0.1400313(72)	9.00(27)	−24.2(4.2)	1.1814(69)	−10.85(46)	100.3(6.5)	0.34	0.1390
1.78	0.139792(12)	7.60(69)	−8(24)	1.233(14)	−11.2(1.9)	103(71)	3.36	0.1390
1.79	0.139555(13)	6.52(52)	−7(17)	1.287(11)	−12.04(92)	142(24)	0.92	0.1390

[1] F. R. Brown, F. P. Butler, H. Chen, N. H. Christ, Z. h. Dong, W. Schaffer, L. I. Unger, and A. Vaccarino, Phys. Rev. Lett. **65**, 2491 (1990).
[2] R. D. Pisarski and F. Wilczek, Phys. Rev. D **29**, 338 (1984).
[3] S. Gavin, A. Gocksch, and R. D. Pisarski, Phys. Rev. D **49**, R3079 (1994).
[4] C. Schmidt and S. Sharma, J. Phys. G: Nucl. Part. Phys., DOI: 10.1088/1361-6471/aa824a (2017).
[5] H. T. Ding, *Proc. Sci.*, LATTICE2016 (2017) 022.
[6] S. Aoki *et al.* (JLQCD Collaboration), Nucl. Phys. B. Proc. Suppl. **73**, 459 (1999).
[7] F. Karsch, E. Laermann, and C. Schmidt, Phys. Lett. B **520**, 41 (2001).
[8] P. de Forcrand and O. Philipsen, J. High Energy Phys. 01 (2007) 077.
[9] D. Smith and C. Schmidt, *Proc. Sci.*, LATTICE2011 (2011) 216.
[10] P. de Forcrand, S. Kim, and O. Philipsen, *Proc. Sci.*, LATTICE2007 (2007) 178.
[11] G. Endrodi, Z. Fodor, S. D. Katz, and K. K. Szabo, *Proc. Sci.*, LATTICE2007 (2007) 182.
[12] H.-T. Ding, A. Bazavov, P. Hegde, F. Karsch, S. Mukherjee, and P. Petreczky, *Proc. Sci.*, LATTICE2011 (2011) 191.
[13] A. Bazavov, H.-T. Ding, P. Hegde, F. Karsch, E. Laermann, S. Mukherjee, P. Petreczky, and C. Schmidt, Phys. Rev. D **95**, 074505 (2017).
[14] Y. Iwasaki, K. Kanaya, S. Kaya, S. Sakai, and T. Yoshie, Phys. Rev. D **54**, 7010 (1996).
[15] X. Y. Jin, Y. Kuramashi, Y. Nakamura, S. Takeda, and A. Ukawa, Phys. Rev. D **91**, 014508 (2015).
[16] X.-Y. Jin, Y. Kuramashi, Y. Nakamura, S. Takeda, and A. Ukawa, *Proc. Sci.*, LATTICE2015 (2015) 160.
[17] S. Takeda, X. Y. Jin, Y. Kuramashi, Y. Nakamura, and A. Ukawa, *Proc. Sci.*, LATTICE2016 (2017) 384.
[18] Y. Iwasaki, Report No. UTHEP-118, 1983.
[19] S. Aoki *et al.* (*CP*-PACS and JLQCD Collaborations), Phys. Rev. D **73**, 034501 (2006).
[20] Y. Nakamura and H. Stuben, *Proc. Sci.*, LATTICE2010 (2010) 040.
[21] M. A. Clark and A. D. Kennedy, Phys. Rev. Lett. **98**, 051601 (2007).
[22] Y. Kuramashi, Y. Nakamura, S. Takeda, and A. Ukawa, Phys. Rev. D **94**, 114507 (2016).
[23] A. M. Ferrenberg and R. H. Swendsen, Phys. Rev. Lett. **61**, 2635 (1988).
[24] M. Lüscher, J. High Energy Phys. 08 (2010) 071; 03 (2014) 92(E).
[25] S. Borsanyi *et al.*, J. High Energy Phys. 09 (2012) 010.
[26] P. de Forcrand and M. D'Elia, *Proc. Sci.*, LATTICE2016 (2017) 081.